Journal of Fusion Energy (2023) 42:45
https://doi.org/10.1007/s10894-023-00373-9

ORIGINAL RESEARCH

# Physics and Technology Research for Liquid-Metal Divertor Development, Focused on a Tin-Capillary Porous System Solution, at the OLMAT High Heat-Flux Facility

A. de Castro[1] · E. Oyarzábal[1] · D. Alegre[1] · D. Tafalla[1] · M. González[1] · K. J. McCarthy[1] · J. G. A. Scholte[2,3] · T. W. Morgan[2,3] · F. L. Tabarés[1] · and the OLMAT team

Accepted: 1 August 2023 / Published online: 4 September 2023


**Abstract**
The operation of the Optimization of Liquid Metal Advanced Targets (OLMAT) facility began in April 2021 with the scientific objective of exposing liquid-metal plasma facing components (PFCs) to the particle and power fluxes provided by one of the hydrogen neutral beam injectors of the TJ-II stellarator. The system can deliver heat fluxes from 5 to 58 MW $m^{-2}$ of high energy hydrogen neutral particles ($\leq$ 33 keV) with fluxes up to $10^{22}$ $m^2$ $s^{-1}$ (containing an ion fraction $\leq$ 33% in some instances), pulsed operation of 30–150 ms duration and repetition rates up to 2 $min^{-1}$. These characteristics enable OLMAT as a high heat flux (HHF) facility for PFC evaluation in terms of power exhaust capabilities, thermal fatigue and resilience to material damage. Additionally, the facility is equipped with a wide range of diagnostics that includes tools for analyzing the thermal response of the targets as well as for monitoring atomic/plasma physics phenomena. These include spectroscopy, pyrometry, electrical probing and visualization (fast and IR cameras) units. Such particularities make OLMAT a unique installation that can combine pure technological PFC research with the investigation of physical phenomena such as vapor shielding, thermal sputtering, the formation/characterization of plasma plumes with significant content of evaporated metal and the detection of impurities in front of the studied targets. Additionally, a myriad of surface characterization techniques as SEM/EDX for material characterization of the exposed PFC prototypes are available at CIEMAT. In this article, first we provide an overview of the current facility upgrade in which a high-power CW laser, that can be operated in continuous and pulsed modes (0.2–10 ms), dump and electrical (single Langmuir) probe embedded on the target surface have been installed. This laser operation will allow simulating more relevant heat loading scenarios such as nominal steady-state divertor heat fluxes (10–20 MW $m^{-2}$ in continuous mode) and transients including ELM loading and disruption-like events (ms time scales and power densities up to GW $m^{-2}$ range). The work later focuses on the more recent experimentation (2022 fall campaign) where a 3D printed Tungsten (W) Capillary Porous System (CPS) target, with approximated 30 μm pore size and a 37% porosity and filled with liquid tin. This porous surface was a mock-up of the PFC investigated in the ASDEX Upgrade divertor manipulator. The target composed with this element was eventually exposed to a sequence of shots with the maximum heat flux that OLMAT provides (58 $\pm$ 14 $MWm^{-2}$). Key questions as resilience to dry-out and particle ejection of the liquid metal layer, its refilling, the induced damage/modification of the porous W matrix and the global performance of the component are addressed, attempting to shed light on the issues encountered with the PFC at tokamak scale testing.

**Keywords** Liquid metal divertor · Plasma-surface interaction · High heat flux facility · Capillary Porous System · Tin

## Introduction

Within the crucial research in the attempt to develop magnetic confinement fusion as a viable energy source for the future, the need for mandatory power exhaust through plasma facing components (PFCs) represents an

See full list of contributors in: F. L. Tabarés, E. Oyarzábal, D. Alegre et al., Fusion Eng. Des. 187 (2023) 113373.

Extended author information available on the last page of the article

outstanding scientific and technological challenge. During the plasma operation of a potential thermonuclear device, the PFCs will need to withstand heat loads and power densities that will challenge the physical constraints and properties of all known solid materials. Tungsten (W) is the material choice for the ITER divertor and, at least within the EUROfusion program, it is also the first option for future demonstration devices based on the tokamak configuration, i.e., DEMO. Its exceptional thermo-physical properties and low sputtering yield under ion bombardment are translated into a nominal perpendicular power load limit that is set at 10 MW $m^{-2}$ for ITER [1], this being reduced to 5 MW $m^{-2}$ in DEMO due to the deleterious effect of the more stringent neutron loading [2].

In order to accomplish these power load limits for the W divertor and also maintain the sputtered high-Z impurity influx below the radiative collapse limits [3], intense divertor plasma detachment [4] and (higher Z impurity induced) core radiation [2] will be needed to volumetrically mitigate a major part of the power exhaust. DEMO baseline scenarios [5] compatible with acceptable sputtering (basic to assure proper PFC lifetime and acceptable W content in the core) will imply a cold plasma edge ($T_e \sim$ 5 eV in front of the W target plates) and a very high power radiation fraction ($f_{rad} \geq 95\%$), induced by seeding of impurities in both edge (divertor) and core plasma. Gyrokinetic predictions have assessed that turbulent spreading can determine larger divertor heat flux widths [6] than the projected by the empirical Eich scaling [7]. Such prediction would result in the amelioration of the previously mentioned $\geq 95\%$ radiation fraction levels, values that appear absolutely unprecedented and challenging from the experimental point of view, to a level around 80%. Nonetheless, such benefit would be produced at the expense of an increase in the parallel heat flux that will make more difficult the constraint of maintaining the electron temperature in front of the targets within the mentioned sputtering tolerable thresholds. In any case, these high $f_{rad}$, low Te, W divertor DEMO baseline scenarios and their snug operational margins are yet to be experimentally validated, being not clear if they will be able to make compatible the mitigated perpendicular heat fluxes to the divertor tiles with the technological limits of the current single-null W monoblock solution [8] and with the programed thermonuclear performance. Obviously, the considerable impurity seeded level will affect fuel concentration and confinement in the core, thus needing a careful monitoring and an extremely efficient control to avoid H-L mode transitions or radiative collapses, in order to ensure operation with the expected thermonuclear gain also preventing from irreversible damage to the divertor elements.

Last but not least, undesired transient events (ELMs, VDEs, disruptions…) will surpass the previously explained nominal heat loading up to levels in the range of GW $m^{-2}$ in timescales of milliseconds. Such a critical aspect will increase/accelerate the progressive deterioration of W elements. This question will decisively affect the lifetime of the W PFCs, whose minimum lifetime, from an economic viability point of view, is set at two years [9]. Among these events, disruptions will be the most hazardous as the associated peak loading can reach $\sim$ 100 GW $m^{-2}$ [10] and provoke catastrophic damage to the W divertor elements. A disruption-induced major failure in the divertor will result in a severe lifetime reduction, probably entailing the unavoidable replacement of the involved elements during machine shutdown. The frequency of this replacement will be crucial for the feasibility of this divertor solution, being generally a key aspect for the availability of any projected fusion power plant [9].

Under such an uncertain scenario, where it cannot be guaranteed that W-based divertor elements will properly satisfy the DEMO power exhaust demands, both in technical and economic terms, the search for alternative solutions is therefore necessary. Liquid Metal (LM) plasma facing components (PFCs), in particular tin, may potentially increase power handling limits beyond W capabilities. It also offers an option that can be more resilient to transients [11] and eventually lengthen the PFC lifetime, these being points that critically effect the economy of a power plant [12]. In such configurations, the liquid surface exposed to plasma possesses intrinsic self-healing and self-replenishment characteristics, while also being virtually immune to permanent neutron damage and protecting the underlying armor from plasma exposure [13], question especially crucial in the case of major transient events that will be fatal for a solid PFC if no sacrificial layers (i.e. liquid metal surface) are able to mitigate it.

Up to date, however, LM PFC solutions possess a clearly lower Technological Readiness Level (TRL) when compared to the more developed and straightforward solid W option. Additionally, the testing of such prototypes in magnetically confined devices obviously results more complex. Previous technological development/validation under linear plasma devices and high heat flux (HHF) facilities is required to optimize and choose the best configurations to be utterly tested at fusion device scale. Usually, these facilities use electron, ion, neutral or laser beams as well as linear plasmas to simulate the divertor heat loading of a fusion device. Many of them are mainly, and frequently only, focused on postmortem analysis of the damaged samples, examining their resilience and power loading threshold to irreversible material deterioration, but otherwise ignoring physics questions related to the interaction of plasmas with a LM PFC.

In this article, first, we provide a brief overview of the OLMAT HHF facility, devoted to studying the physics and technology of LM PFCs. In particular, we focus on its most recent upgrade in which a high-power constant wave (CW) laser, that can be operated in continuous or pulsed modes (0.2–10 ms). This laser will allow simulating relevant heat loading scenarios including nominal steady-state divertor heat fluxes (10–20 MW $m^{-2}$) and transients such as ELM loading and disruption-like events (ms time scales and power densities up to GW $m^{-2}$). Thereafter, the work here is centered on results from the most recent OLMAT experimental campaign (fall 2022). During that campaign a single Langmuir Probe, embedded in a Titanium-Molybdenum-Zirconium (TZM) target, enabled measurements of electron density ($n_e$) and temperature ($T_e$) to be made. In addition, we report on the installation and first trials with the mentioned CW laser and associated subsystems. Indeed, tests were successful in both continuous and pulse modes. The campaign finished with the exposure of a 3D printed CPS W porous target (30 μm of average pore size) filled with liquid tin to OLMAT pulses. This CPS structure is a mock-up of the prototype investigated in the ASDEX Upgrade divertor manipulator [14] and it was exposed eventually to a sequence of shots at the maximum power load that the system provides (58 ± 14 MW $m^{-2}$). Key questions such as resilience to LM surface dry-out and the ejection of as particles or droplets from the liquid metal layer, its refilling, induced damage/modification of the porous, underlying W matrix, and the global performance of the component are addressed in an attempt to shed light on the issues encountered with this PFC option at tokamak scale testing.

## Experimental Description

### Brief Portrayal of the OLMAT HHF Facility, Experimental Capabilities and Endeavors Carried Out Within the 2022 Fall Campaign

The operation of the OLMAT (Optimization of Liquid Metal Advanced Targets) HHF facility began in April 2021 with the scientific objective of exposing Liquid-Metal (LM) PFCs to particle and power fluxes provided by one of the two hydrogen Neutral Beam Injectors (NBI) of the TJ-II stellarator. This system can provide heat fluxes from 5 to 58 MW $m^{-2}$ of high energy hydrogen neutral particles ($\leq$ 33 keV) with fluxes in the range of $10^{22}$ $m^{-2}$ $s^{-1}$ (containing an ion fraction $\leq$ 33%) in a pulsed operation of 30–150 ms duration and frequencies up to 2 $min^{-1}$. This 33% ion fraction on the primary beam in foreseen in order to increase the power load of the shot beyond 40 MW $m^{-2}$ by deactivating the bending magnet that deflects the non-neutralized ions of the neutral beam before entering into the duct. In this way, the total flux of energetic particles reaching the target increases with maximum achievable power loads of 58 ± 14 MW $m^{-2}$. These characteristics define OLMAT as a high heat flux (HHF) facility for PFC evaluation in terms of power exhaust capabilities, thermal fatigue, and resilience to material damage. A fully detailed description of the conceptual design of the OLMAT facility, its commissioning and first results can be found in previous papers [15, 16].

The facility is equipped with a wide range of thermal, optical, and plasma diagnostics as well as visualization tools. Among them, there are systems for analyzing the thermal response of the targets: 2 infrared (IR) pyrometers (OPTRIS CTlaser and OPTRIS 3MH1 measuring at 1.6 μm) as well as one IR camera (Optris PI 160 measuring in the range of 7.5–13 μm). For monitoring of atomic/plasma physics and plasma-surface interaction phenomena within the created plasma plume in front of the exposed surface, the system is equipped with two spectroscopy instruments: a CMOS-based spectrometer (compact fiber optic covering the 236–812 nm range) and a 16-channel photomultiplier array (Hamamatsu, mod: R5900U-L16) alternatively equipped with a tin (452.5 nm)/Hα (656.3 nm) filter. This array is tangentially aligned to view the exposed target and can collect the spatial distribution of the emission lines. The spectroscopic units provide basic data to infer tin erosion (physical and thermal sputtering as well as evaporative influx) as well as possible sputtering from the underlying W matrix (real time indicator of local dry-out of the LM surface). Electric units (properly isolated connections) to collect the global floating potential/saturation current of the complete surface exposed to the beam are inserted through the backside of the target. Finally, a compact, fast-camera (AOS PROMON U750 mono) is also used to record the evolution of the exposed surface and created plasma plume during the experimental pulses, also tracking surface inhomogeneity, the possible formation of liquid leakages in the liquid tin surface during/after exposure, and liquid droplet/particle ejection during the shots.

The above systems make OLMAT an unique HHF installation that may combine pure technological LM PFC research with the investigation of physical phenomena such as vapor shielding, thermal sputtering, radiative dissipation of incoming heat fluxes and the formation/characterization of LM-enriched plasma plumes. In Fig. 1, a bird's eye view sketch is present that visualizes the facility configuration, target, and beam placement as well as the positioning of the optical viewing ports in through which lines of sight of the different diagnostics are aligned. The diagnostic configuration sketched in Fig. 1 is the most frequent set-up. Nonetheless some flexibility within the

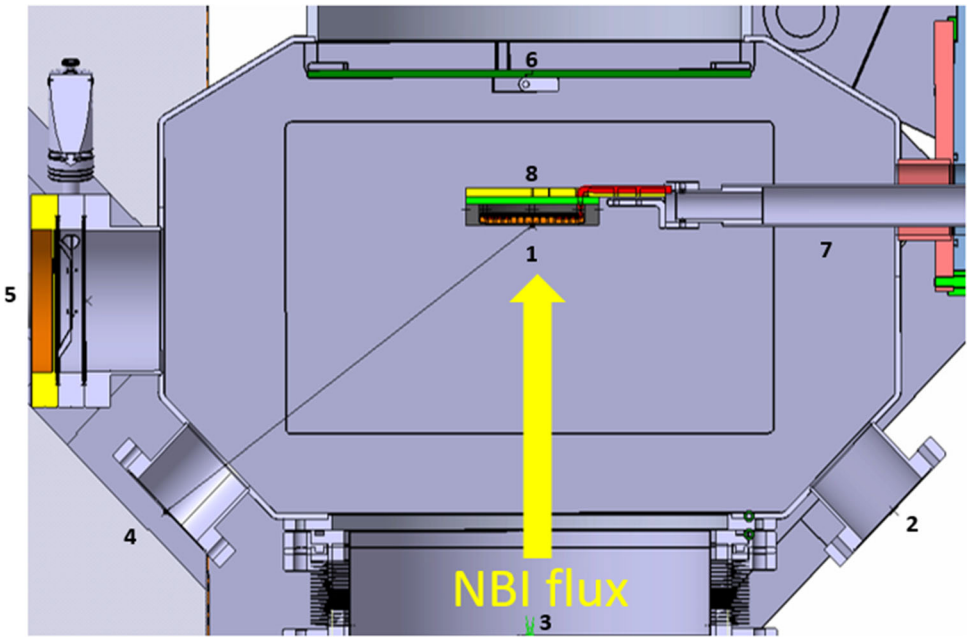


**Fig. 1** Top view sketch of the OLMAT experiment. (1) Front surface of the target exposed to the neutral particle beam and associated heat loads. (2) Optical port view for IR pyrometers and cameras. (3) Neutral beam injector duct. (4) Optical port view for the CMOS-based spectrometer (236–812 nm range) and compact fast camera. (5) Optical port view (tangential to the target) for a 16-channel photomultiplier array equipped with a tin/Hα filter. (6) Titanium–Molybdenum–Zirconium (TZM) alloy shield for protecting the gate valve that couples OLMAT to the main chamber of TJ-II stellarator. (7) Manipulator with rotation/translation capabilities for the exposed target. (8) Back side of the studied target where thermocouples, heating elements and electrical probing system (whole surface floating potential/saturation current probe or specific single Langmuir probe for local characterization) are inserted

diagnostic placement is possible when required. Given the limited space for this article, for additional sketches or 3D CAD views, the reader is referred to [15, 16]. Finally, a myriad of surface characterization techniques for material and surface science characterization of the exposed targets are available at the laboratories of the Fusion Technology Division of CIEMAT. In this work, Scanning Electron Microscopy and Energy Dispersive X-Ray Spectroscopy (EDX) has been utilized for such purpose. Three different scientific/technical activities have been performed within the 2022 fall OLMAT campaign. They are outlined in the next subchapters.

### Installation and First Trials with the High Power CW Laser

The second upgrade entailed the installation, tuning, and operation starting phase of the CW Y laser (YLS-900/9000-U-QCW model provided by Photonics) of 90 J energy ($\lambda$ = 1061 nm). This laser may be operated in pulsed or continuous mode with power characteristics of 930 W in continuous and 9300 W when pulsed (0.2–10 ms length). In the case of incident wavelength of 1.06 microns, the optical reflectivity coefficient for liquid tin between melting point and 465 °C is 77% [17], resulting in maximum absorbed power loads of 214 and 2140 W for continuous and pulsed mode operation respectively. The spot size (ellipsoidal shape as its angle of incidence with the target is 52°) and associated power densities will depend on the combination of focus length and distance to the target (the laser head is on a movable stage) of the specific lens coupled to the laser head. In this way power densities ranging from steady state, to slow transients until fast, high energy transients such as disruption-like events may be simulated just moving the laser head.

The planned operation within the continuous mode can include ITER-DEMO nominal divertor-like pulses with power densities in the range of 10 MW $m^{-2}$. The potential duration may range from few seconds (until reaching thermal steady state) up tens/hundreds of seconds. Additionally, divertor reattachment (slow transients) can be simulated in this mode with power densities varying in the range of 20–70 MW $m^{-2}$ (or even larger, being the upper limit for tin targets around 350 MW $m^{-2}$ for a finely focused spot around 0.5 $mm^2$). Additionally, synergetic effects derived from the simultaneous exposition of PFC prototypes to the NBI beam of OLMAT and the laser can be also explored.

With pulsed mode, the shot duration will be in the range of typical magnetic fusion device instabilities (0.2–10 ms, with a total, injected energy of 90 J). The frequency of the shots can be varied within the range of 10–2000 Hz. This is also in the order of type III ELMs where the effects of

thermal fatigue can be mimicked. For disruption simulation, in the case of a tin surface, proper focusing would allow providing power loads up to 3.5 GW $m^{-2}$ deposited in 1–4 ms on a 0.5 $mm^2$ spot.

Several trials were performed with the laser in both continuous and pulsed modes. It should be noted that, during the continuous mode tests, a W CPS target filled with liquid tin was exposed to several shots with durations of tens of seconds. These trials with the Sn-filled target were successful in terms of irradiation and in situ diagnosis of the target but revealed technical issues related to the (continuous) heating of the optical window (symbolized with number 4 in Fig. 1) that need to be solved. Additionally, the laser spot and its spatial profile were characterized in order to corroborate its expected characteristics (Gaussian profile). The energy of the laser beam, focused with a f = 250 mm lens, was measured with a High Energy Pyroelectric Sensor (OPHIR PE50BF-DIFH-C) placed at a distance of 13 cm from the laser head exit. The results of these measurements are shown in Fig. 2. It reveals a spot diameter of ≈ 10 mm with a full width at half maximum (FWHM) of 4,25 mm. This basic characterization will allow the extrapolation of more focused spots for the transient load simulation operation. Completion of security requirements and full commissioning of the laser system is planned for 2023 spring. Thereafter, the laser will be fully operative for the experimental campaigns.

## Experimental Activities with TZM Target Containing an Embedded Single Langmuir Probe

With the goal of extending deeper the complex characterization of the plasma plume created in front of an exposed target surface, a specific TZM-based target equipped with an embedded single Langmuir probe (placed at the center) was installed in the lateral manipulator of OLMAT (labelled 7 in Fig. 1) and exposed to NBI shots. It consisted of a TZM target with an isolated (by a boron nitride cylinder) W tip attached at the center of the target. A photo of the LP assembly protruding from the TZM target is shown in Fig. 3.

## Testing of the 3D Printed W Capillary Porous System Target Filled with Liquid Tin (ASDEX Upgrade CPS Mock-Up)

The original 3D-printed porous matrix was provided by DIFFER and was analog to the specimen tested at the divertor of ASDEX Upgrade tokamak [14]. It consisted of a circular disk (diameter of 32 mm of diameter) fabricated through selective laser melting (SLM) at DUNLEE, where the 1.5 mm thickness porous W layer is directly attached to a solid W (lower part of the CPS and non-exposed during the experiments) with equal thickness and diameter. The resulting porous surface with an average pore size of 30 μm and 37% porosity was wetted with liquid tin at the plasma-wall interaction laboratory of CIEMAT. The 3D printed W CPS configuration did not contain an internal, specific reservoir placed beneath the internal porous structure for the liquid percolated tin. The wetting procedure was carried out in a high-temperature vacuum oven. After its cleaning with hydrochloric acid, the 3D printed porous matrix, attached to a TZM annular disk, was placed in the oven with several solid thin Sn (high purity of 99%) slices placed on top of the W surface as can be seen in Fig. 4. The total amount of added tin was around 4 g for an expected thickness of liquid metal ≈ 1.5 mm within the

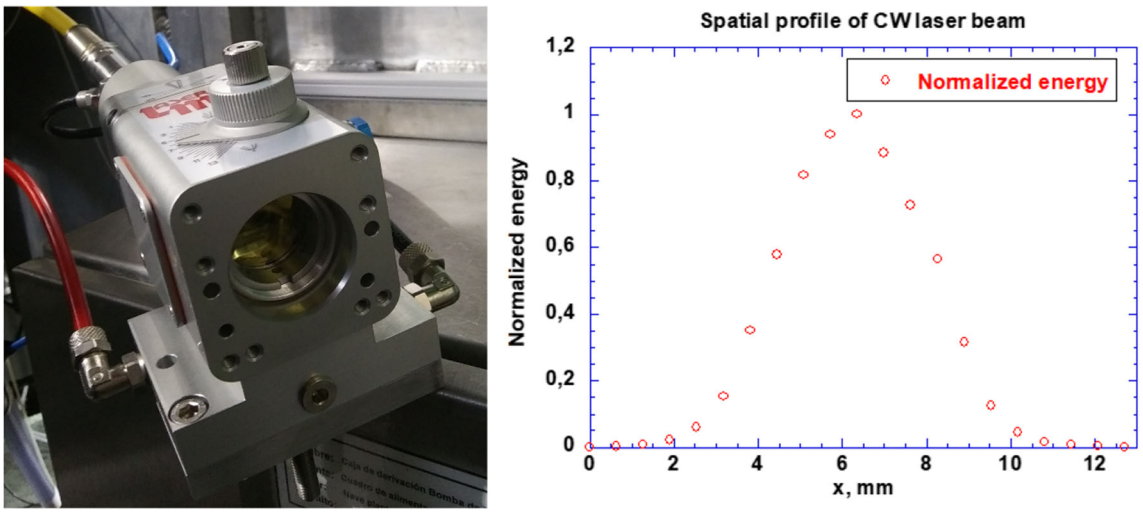


**Fig. 2** Left: laser head. Right: spatial profile of the CW laser beam normalized energy at a distance of 13 cm from the laser head (beam focused with f = 250 mm lens)

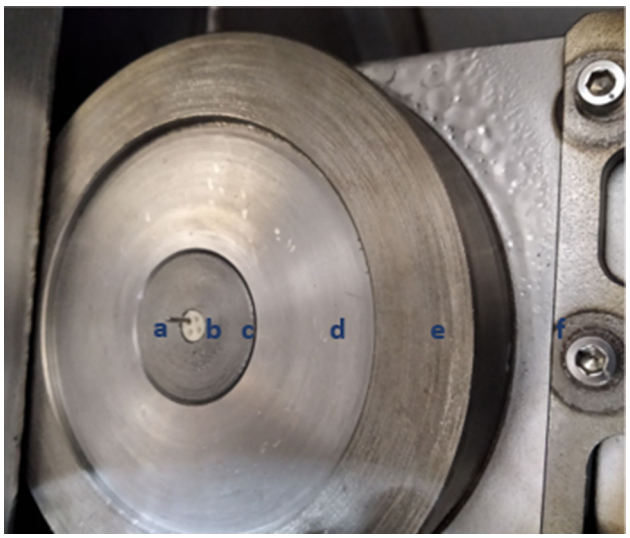


**Fig. 3** Photo of the TZM-based target (prior to its insertion into the main OLMAT chamber via the connection valve coupled to the pre-chamber) with a single Langmuir probe embedded at its center. From the center to the right side: **a** W probe tip, **b** boron nitride insulator, **c** inner annular TZM disk, **d** outer annular TZM disk, **e** TZM target mask, **f** connection to the target manipulator for lateral translation

CPS. Then the air in the oven is pumped out to a base pressure of 5 mTorr. Next, the oven was progressively heated up to 1150 °C (heating ramp of 100 min) and was then kept at this temperature for 3 min before being inertially cooled down to room temperature. The visual inspection after the wetting process revealed a CPS substrate fully wetted by a tin brighter layer, being the porous structure completely filled as well as showing the spreading of the excess Sn beyond the CPS edges. Due to the modest vacuum level achieved, the formation of oxide layers (darker spots shown in Fig. 4, right) on the top of the Sn wetted area was unavoidable. After this preparation, the tin-covered CPS was attached to the target, installed in the lateral manipulator and inserted into the OLMAT chamber which was pumped out and prepared for the experimental sessions.

## Experimental Results and Discussion

### TZM Target with a Single Embedded Langmuir Probe to Characterize Plasma Parameters

The extreme thermal loading operation was conducted at progressively increasing power loads and pulse duration, i.e., 5–58 MW $m^{-2}$ and 50–100 ms, while collecting multiple I–V characteristic curves during each shot duration. The cylindrical probe tip (length of 4.75 mm and diameter of 0.75 mm) was fed with ± 14 V repetitive biasing cycles. During operation at the highest power loads, the probe tip was partially damaged/melted, but it continued working and collecting I–V data. From the data, absolute values for the electron temperature (from the I–V

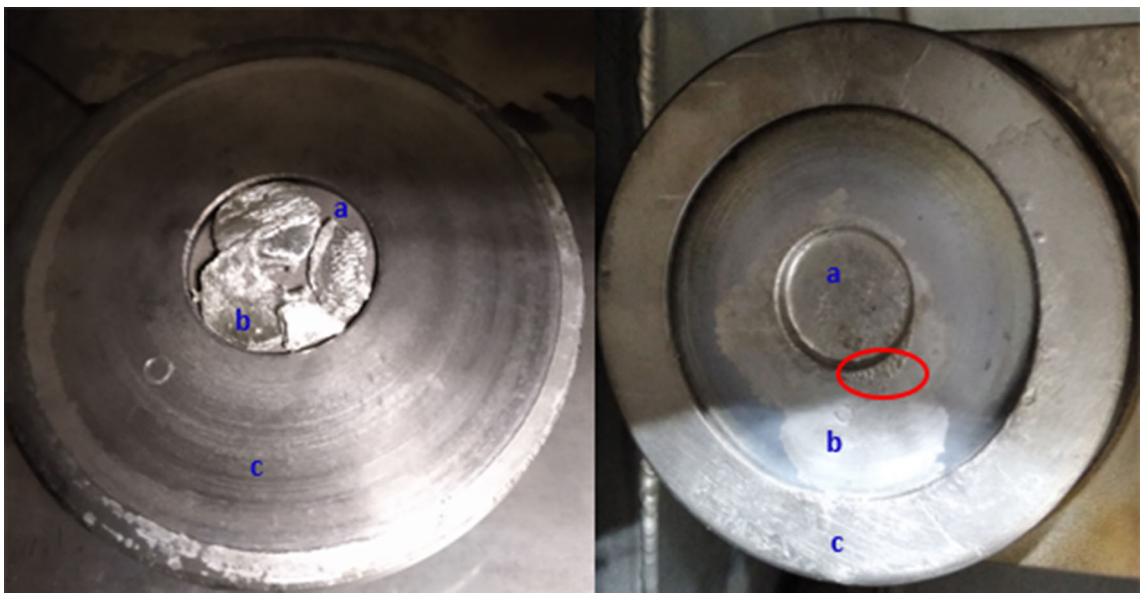


**Fig. 4** Photos of the Sn–W CPS (ASDEX Upgrade CPS mock-up) target during different moments prior to its testing at OLMAT. Left: specimen prepared for the wetting procedure, **a** original W 3D printed matrix, **b** thin tin slices, **c** TZM annular disk. Right: Sn-filled CPS element assembled and placed on the lateral manipulator just before being introduced in the OLMAT main chamber, **a** Sn-wetted CPS surface where dark spots (likely oxide layers) are visible, **b** TZM annular disk, TZM target mask. On the right side picture, close to the boundary between regions (**a**) and (**b**), tin deposits (marked with a red oval), caused by its liquid spreading beyond the CPS surface during the wetting procedure, can be appreciated

slope) and density (from ion saturation current) of the created plasma cloud (mainly containing hydrogen species reflected from the main neutral beam but also some molybdenum, originated by sputtering, as well [16]) over time were deduced for the different shots varying in power load and total particle fluence. According to first estimates, electron density measurements from $5 \times 10^{17}$ to $5 \times 10^{18}$ $m^{-3}$ and temperatures in the range of 3–11 eV were obtained depending on power density, pulse duration, ion content of the NBI beam and relative time of the I–V scan. Due to the uncertainties in the determination of ion saturation current and the error associated to the fitting, statistics, data acquisition and treatment as well as error propagation, in some instances the global error bars associated to the density measurements accounted up to a 40–50% factor. The obtained $n_e$ and $T_e$ values at t = 1042 ms (close to the discharge end that is set at t = 1050 ms) are shown in Fig. 5 for the case of OLMAT shots containing a significant ion fraction (up to 33%) and power densities varying from 10 to 58 MW $m^{-2}$. The results and probe interpretation were possibly affected by thermionic emission at higher power densities, thus perturbing the I–V measurements and hence the deduced parameters. These first endeavors with the simpler case of a solid TZM target were intended as an initial proof of concept within the OLMAT experiment, projecting to extrapolate the methodology to LM-based CPS targets where more challenging technical and interpretation issues will be encountered for the diagnosis of plasmas with significant content of evaporated/sputtered liquid metal atoms. In the 2023 spring campaign the technique was successfully extended to a W–Sn CPS target (W felt covered by liquid tin) being the related data under analysis and likely content of a separate, future paper.

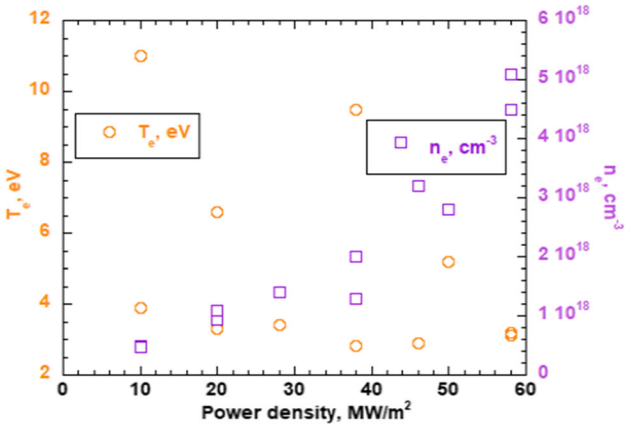


**Fig. 5** $T_e$ and $n_e$ values of the plasma plume created in front of the solid TZM target for OLMAT shots containing a significant ion fraction (up to 33%) with duration of 50 ms and varying in power density. These measurements were taken at t = 1042 ms (with discharge finishing at t = 1050 ms). Error bars for density may account (specially at lower densities) up to a 40–50% of the measurement due to the uncertainties on data fitting/collection, statistics, error propagation and determination of saturation currents. Error bars for the electron temperature values were in the range of 5-10 % due to the error associated to the statistical fitting. Both error bars are not shown in the Figure to favor the visualization of the obtained values for electron temperature and density

## Experimentation with the 3D Printed W–Sn CPS Prototype (ASDEX Upgrade CPS Mock-Up)

The total exposure of this target to the OLMAT beam during the different experimental sessions accounted 203 OLMAT shots including 35 of 100 ms length containing the maximum achievable power load of 58 ± 14 MW $m^{-2}$ and associated $F_{HF}$ =19 MW $m^{-2}$ $s^{-1/2}$. During the first experimental session, the LM PFC was exposed to progressively increasing power loading (5–58 MW $m^{-2}$). As commented in subsection 2.4, after the wetting procedure, the target presented an excess of tin in some regions (Fig. 5 right) in the form of solid deposits and also dark spots probably containing oxides. The exposure of the target to the first 10–20 shots (varying power loading between 5 and 10 MW $m^{-2}$ and shot duration between 30 and 100 ms) demonstrated to be an efficient wall conditioning capable of cleaning up the passivated layers (most likely oxides). After that, during the first shot with 100 ms duration and power load of around 20 MW $m^{-2}$, the fast camera observed the leakage, sliding and dropping of the excess liquid Sn from the CPS surface. Figure 6 (left) shows a caption from a fast camera video at the moment in which a portion of liquid tin detaches from the vertical CPS surface. Once this macroscopic excess of liquid metal was released, massive ejections were no longer observed during the experimental sessions. This observation points that the combination of high surface tension and viscosity as well as the limited wettability of tin on adjacent areas may result in the wicking and spelling of the excess of molten metal detected in the experiment, showing that the CPS surface was incapable of confining this liquid metal excess by means of capillary force. Although not in a vertical position (the analog Sn CPS tile was placed within the divertor in a horizontal position) this kind of issue (leakage of Sn from the CPS surface edges) has been also inferred during experiments performed at ASDEX Upgrade [14], not directly observed in real-time, though. The phenomenon constitutes a main source of tin impurities that strongly affect the plasma performance in fusion devices and will require inhibition strategies for Sn CPS implementation at tokamak scale.

After this first session, the PFC was exposed to 2 sequences of 50 discharges with power load around 10 MW $m^{-2}$ and 100 ms, of duration with a frequency

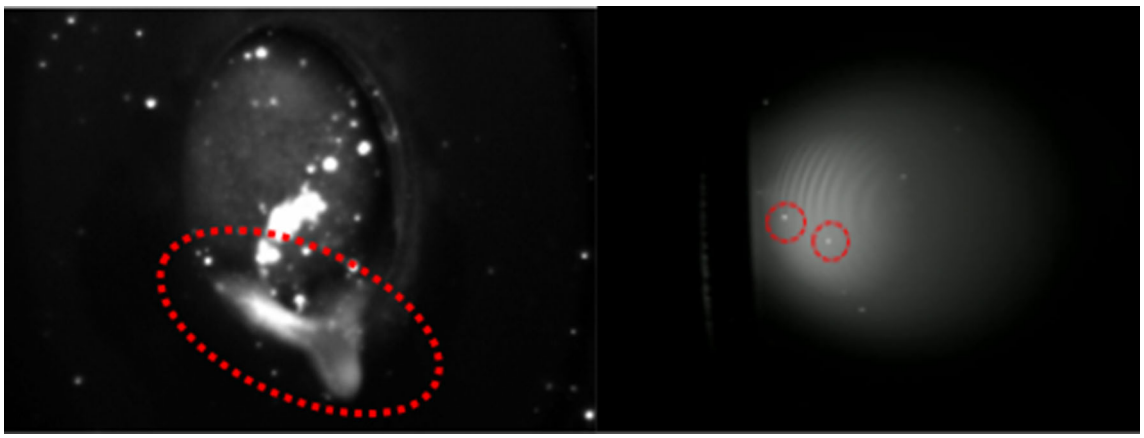

**Fig. 6** Images taken from a series of fast-frame camera videos. Left−Frontal image of the CPS element (at the center) at the moment when the excess of liquid tin leaks (highlighted with a dotted red oval) from the CPS surface and falls vertically. Right−Lateral (tangentially oriented to the target) video with a Sn transmission filter, for the last OLMAT shot with maximum power of 58 ± 14 MW $m^{-2}$ and pulse duration of 100 ms. The target edge (black rectangular contour) is visible on the left. To its right, at the image center, a spherical plasma plume that has evolved from the liquid Sn surface and contains several droplets/particles (bright circular spots with an approximated few mm diameter) that were released from the LM target surface. Two of them are encircled in dotted red within the image

0.67 $min^{-1}$. No indications of PFC damage and/or significant target erosion were recorded during the shots by the visualization tools. Finally, in order to explore the physics of vapor shielding onset and performance limits (in terms of resilience to dry-out) of the PFC, the target was exposed to 27 consecutive discharges with the maximum power of 58 ± 14 MW $m^{-2}$ and pulse duration of 100 ms. These maximum power load shots have an associated Heat Flux Factor ($F_{HF}$) of around 19 MW $m^{-2}$ $s^{-1/2}$ [16]. During these maximum power shots, the final temperature reached by the tin CPS surface was around 1200 °C according to the absolutely calibrated IR pyrometry signal. Additionally, by fitting the corresponding black body radiation spectrum a maximum temperature of 1300 °C on the target surface was estimated. At this temperature level the onset of vapor shielding effects dissipating part of the impinging heat flux was inferred due to the observed deviation (decrease) on the temperature rise with respect to the progressive heating that would correspond to the slab model heat transfer prediction. Full details and analysis about the vapor shielding onset studies will be presented in a future paper, so this chapter is centered on exploring the limits of the target in terms of LM surface dry-out, resilience of the CPS and on the related post-mortem material analyses (SEM-EDX).

During the last shot at the highest power load (carried out at the end of the experimentation with the CPS, after a much larger total hydrogen fluence was loaded on the liquid tin surface), the fast-frame camera, tangentially oriented to the Sn CPS surface and equipped with tin emission line transmission filter, showed the ejection of liquid metal droplet/particles (Fig. 6 right) in the form of bright circular spots with diameter within the mm size range. The phenomenon, previously documented in [18], is believed to be produced by the super-saturation of hydrogen happening inside liquid tin in the form of bubbles that transiently explode, although it is also discussed that the formation of volatile and thermally unstable tin hydride molecules might also play a role in the process. In our experiments, however, the supersaturation of the liquid tin content with hydrogen produced shot by shot cannot be confirmed as the temperature excursion of the CPS during these shots is high enough (≫ 600 °C) to induce intense desorption of hydrogen from the liquid Sn bulk. Therefore, regarding this observed tin particle ejection, the possible influence of other questions as the intense damage in the CPS structure and the concomitant deleterious effect on the effective capillary action cannot be discarded. In any case, this experimental finding constitutes another potential source of high-Z tin impurities at fusion device scale testing that needs to be controlled/minimized. As the experiments in AUG have shown certain levels of tin within the plasma core are translated in a clearly degraded plasma performance [14]. The results presented here demonstrate that, in the absence of a magnetic field, the tin particle ejection happened with this CPS configuration in shots with a duration of 100 ms and power densities of 58 ± 14 MW $m^{-2}$.

Figure 7 shows comparative pictures of the target before and after exposure to the OLMAT thermal loads. As can be seen, as a result of the OLMAT operation, clear signs of tin redeposition/coverage along the target (presence in the center picture of wider and more extended grey layers, mainly composed by tin, within TZM annular masks after OLMAT exposure) are visible. Moreover, as the picture

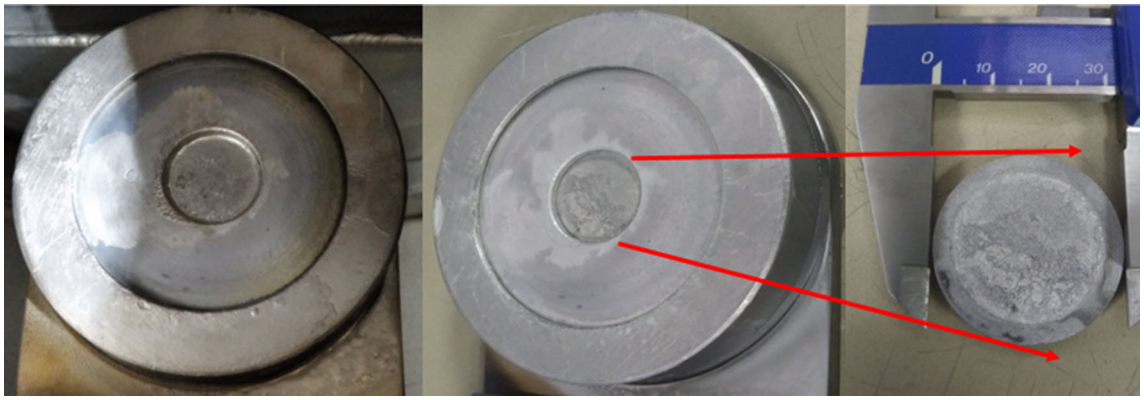

**Fig. 7** Comparative photos of the Sn filled 3D printed W CPS. Left: Picture taken before starting operation at OLMAT (the CPS element is placed at the center of the target and is surrounded by the TZM annular disk and the TZM target mask). Center: Equivalent picture after the OLMAT exposition. Right: Picture of the CPS element after OLMAT exposure and target disassembly, where an irregular Sn layer on the CPS surface is visible after the experimental sessions that finished with 27 repetitive 58 ± 14 MW $m^{-2}$ (100 ms) discharges

placed on the right side of Fig. 7 (taken only on the CPS central portion of the target) shows, in some parts of the CPS the liquid Sn layer was progressively evaporated/eroded, resulting in an irregular surface. Consequently, it seems plausible that during the last highest power density, some regions of the underlying porous W matrix could be directly exposed to the OLMAT beam as a result of the LM layer dry-out.

Two different emission spectrum recorded taken by CMOS-based spectrometer are presented in Fig. 8. These were obtained during the first and last 58 ± 14 MW $m^{-2}$ (100 ms) OLMAT pulses of the 27 repetitive shot sequence. Comparing the spectra, Sn I line emission is clear in both shots, but in the last one, appreciable W I lines (383,5 and 386.8 nm [19]) are present after 27 consecutive discharges thus marking the partial dry-out of the liquid tin surface and the eventual exposition of some parts of the W underlying matrix. This Sn surface dry-out is a result of insufficient LM refilling of the surface and/or liquid tin shortage due to the progressive global erosion.

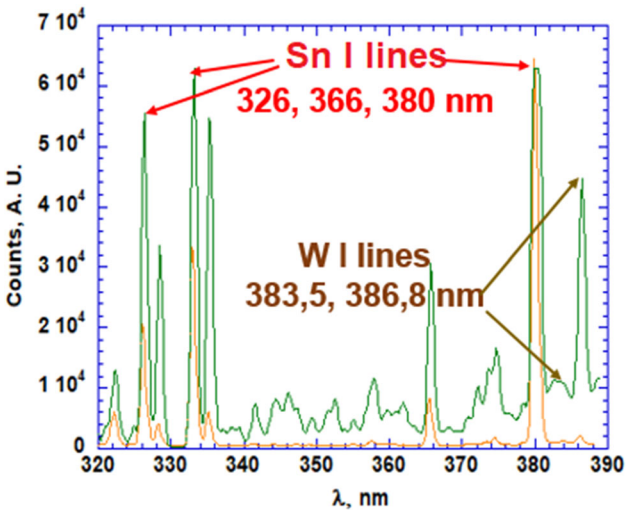


**Fig. 8** Emission spectra collected during the last experimental session. The orange line corresponds to the first 58 ± 14 MW $m^{-2}$ (100 ms) shot of the session while the green one corresponds to the last one with the same power loading. Tungsten I emission lines are present after 27 discharges at the highest power loading as a result of the partial dry-out of the LM surface

For a deeper insight into these dry-out questions and to analyze the surface status and composition of the CPS surface at the microscale, postmortem SEM and EDX techniques were employed (Zeiss Auriga Compact equipment placed at the Fusion Technology Division of CIEMAT). Unfortunately, due to the lack of time, no pre-mortem equivalent analysis was performed either at DIFFER or CIEMAT for sample benchmarking. If time allows, future endeavors contemplate a much more exhaustive and rigorous protocol for the sample characterization, entailing reference analysis after the W 3D printing and the wetting of the porous matrix with Sn. Images from the post-mortem SEM/EDX analyses carried out on the Sn–W CPS target (ASDEX Upgrade CPS mock-up) are found in Fig. 9.

In Fig. 9 left, only the bottom right corner is covered by an Sn foil/flake (with crystal-like structures clearly below 6 μm size marked with the red oval, see next figure). In the rest of this image, the 3D printed W is present (corroborating the inferred real-time dry-out that was spectroscopically detected in Fig. 8). Some larger (less frequent though) crystal-like structures (cubic, tetrahedral) appear also within the 3D printed W filaments, this being a characteristic that was not found in the pre-mortem SEM benchmark carried out within the analog 3D printed W surface that was later wetted with Sn and tested at the ASDEX Upgrade divertor [14]. How such a temporal modification of the W porous structure may potentially

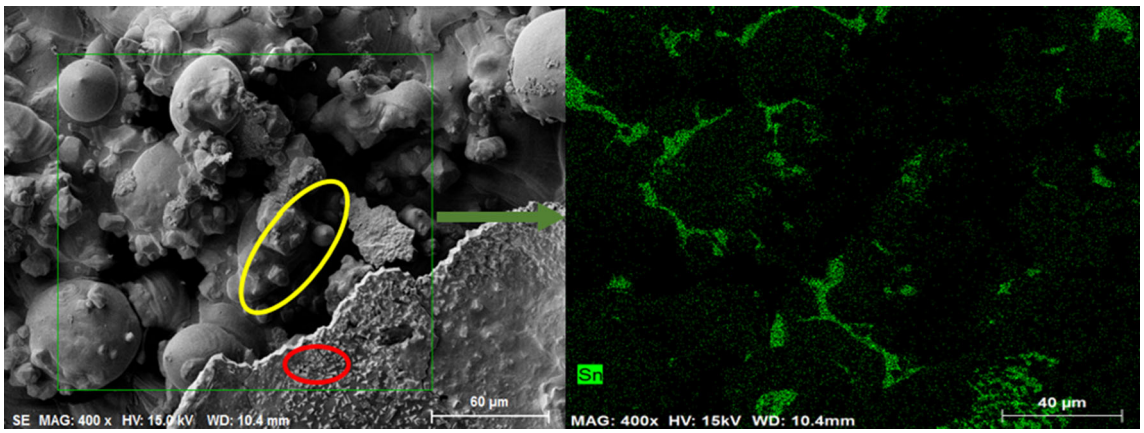


**Fig. 9** SEM and EDX 2D mapping measures performed on the CPS surface exposed at OLMAT. Left: SEM picture in which an irregular tin flake is present at the bottom right corner. A red oval marks a region within this Sn flake (object of study in the next Fig. 10) with micron sized crystal-like structures. The underlying porous W matrix occupies the rest of this image, where regions with cubic and/or tetrahedral-like larger W crystals within the 3D printed W filaments appear to be also visible (marked with yellow oval). Right: 2D EDX mapping for Sn (in green), performed on the square represented on left SEM picture. The black areas correspond to the zones where W is the major constituent after the exposition at OLMAT. Some regions of this exposed W area shows the commented "recrystallized" 3D printed W filaments

affect the surface stability, LM wetting and global performance of these PFC prototypes is, at present, uncertain. It is logical to think that the extreme heat loading operation at OLMAT induced some recrystallization on the W matrix (a process that indeed happens around 1000°C for severely damaged W and 1550 °C for cold rolled W [20]). Nonetheless, it is also true that these patterns could be produced also by a partially defective 3D printing process. Due to the absence of a pre-mortem SEM benchmark on the studied CPS, the definitive origin of these crystal-like structures present on the visible 3D printed W filaments of the matrix cannot be absolutely assured. In Fig. 10 the region marked with a red oval in Fig. 9 left is zoomed and analyzed with more magnification.

At this smaller few micron size scale, the presence of crystal-like structures (where the major constituent is W according to EDX mapping results) is more widely extended, being surrounded by remaining tin layers. After the 3D printing process for the W matrix, these very small crystal structures are difficulty present and much less with the large affluence shown herein, probably indicating that the extreme irradiation at OLMAT at least, drove the multiplication of these defects on the W matrix that was exposed to the NBI beam after liquid tin dry-out. Nevertheless, more exhaustive surface analyses, including more detailed pre-mortem benchmarking and maybe more sophisticated techniques such as X-ray diffraction (XRD) or 2D microscopy are necessary to go deeper into this firstly observed W recrystallization signs in the CPS matrix.

## Summary and Conclusions

After its commissioning, the OLMAT HHF facility is fully operative for the research and development of LM PFCs. Its operation is contributing to shed light on the main drawbacks encountered with liquid tin CPS PFCs at tokamak scale testing. Therefore, the OLMAT facility appears as a relevant testbed for alternative LM PFC testing, selection and validation before its installation in fusion devices as for example future machines like DTT and COMPASS Upgrade Tokamaks that plan to investigate these innovative PFC concepts [21, 22]. As a result of the last facility upgrades, a high-energy CW laser was installed and manually operated, with complete operation/commissioning being scheduled by 2023. Other upgrades in the chamber, access ports and auxiliary systems (target active cooling) are also underway and will eventually enable the exposure of targets containing other LM candidates (lithium, tin-lithium alloys) as well as alternative configurations (flowing, hybrid CPS-flowing) whose possible advantages in terms of compatibility, more benign liquid surface behavior and the potential benefits in plasma confinement/performance at fusion device scale cannot be ignored, being OLMAT fully open to investigate them. On the other hand, the operation with a TZM target holding an

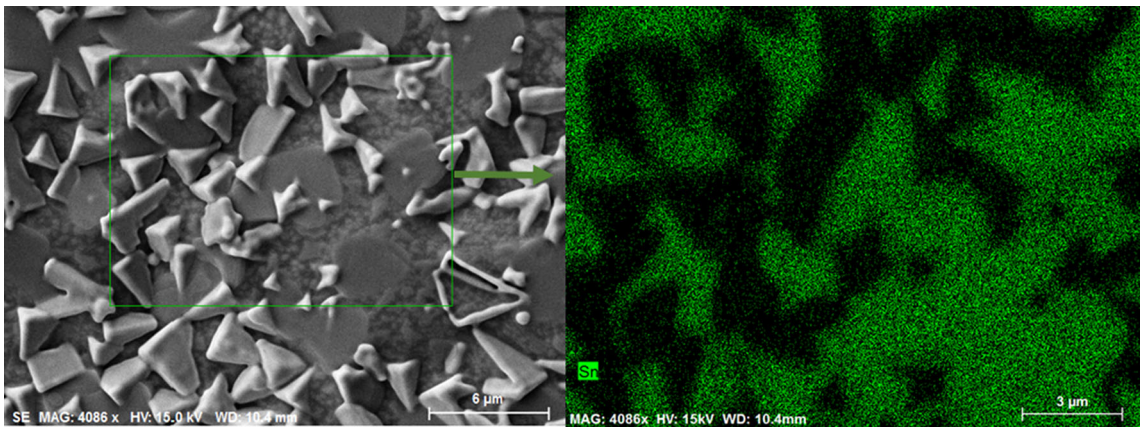


**Fig. 10** SEM and EDS 2D mapping performed on the CPS surface exposed to OLMAT operation at micron size scale. Left: SEM picture where crystal like structures are widely present. Right: Analogue 2D EDX mapping for tin (green color), performed on the green square represented on left SEM picture, where black areas correspond to zones where W is the major constituent, also showing the extended micron-size W recrystallization pattern

embedded single Langmuir probe has enabled characterization of the electron temperature and density of the plasma plume created in front of the target, with time resolution shorter than milliseconds. In the next campaigns, it is planned to be extrapolated to the case of a liquid metal filled CPS target.

Experiments with a tin-filled CPS prototype (analog to the CPS exposed in the divertor of ASDEX Upgrade) entailed its exposure to 203 OLMAT shots, including 35 of 100 ms length containing the maximum achievable power load of $58 \pm 14$ MW $m^{-2}$ and $F_{HF}$ =19 MW $m^{-2}$ $s^{-1/2}$. This research has shed light on the LM technology/engineering issues related to the survival of a LM layer, providing real-time detection of LM dry-out, macroscopic leakage of the liquid tin excess present on the CPS surface and tin particle ejection (mm size) from it, being them main drawbacks encountered at tokamak scale testing. Considering the results obtained in terms of plasma confinement and performance at the tokamak scale with the analog target [14], these liquid tin surface instability phenomena detected at OLMAT can be intimately related to excessive tin contamination found for the ASDEX Upgrade plasmas. Finally, for this CPS surface, an extended re-crystallization pattern (in both few and tens of micron scales) appeared within the exposed W matrix areas that suffered partial LM surface dry-out after the last 27 repetitive OLMAT discharges of 100 ms duration, power load of $58 \pm 14$ MW $m^{-2}$ and associated $F_{HF}$ =19 MW $m^{-2}$ $s^{-1/2}$. Further efforts with the material characterization are necessary to go deeper in the origin, nature and the possible effects on posterior target performance of these recrystallized-like structures found on the W CPS matrix. To combat the dry-out challenge, plans for studying new generation pore geometries with varying diameter/pore size along the cross section are ongoing in order to investigate the optimization of LM refilling, the minimization of the LM erosion and to improve the stability of the liquid tin exposed surface. Regarding all these experimental endeavors through the development of LM PFCs for future fusion devices, the OLMAT HHF facility is open to international collaboration with both public and private partners worldwide.

**Acknowledgements** The authors want to thank I. Voldiner and G. Martín for their valuable help related to the electrical configuration and data acquisition of the Langmuir probe measurements. This work was partially financed by the Spanish 'Ministry of Science and Innovation' under projects ENE2014-58918-R, RTI2018-096967-B-I00 and PID2020-116599RB-I00. This work has been carried out within the framework of the Eurofusion Consortium and has received funding from the Euratom research and training program 2014–2018 under Grant Agreement No. 633053. The views and opinions expressed herein do not necessarily reflect those of the European Commission.

**Author Contributions** AdeC: Conceptualization, Methodology, Validation, Formal analysis, Investigation, Writing−original draft, Writing−review & editing. EO: Conceptualization, Methodology, Validation, DA: Conceptualization (beam dump conceptual design), Methodology. DT: Conceptualization, Methodology, KJM: Conceptualization, Methodology, partial formal analysis (spectroscopy), MG: Conceptualization, Methodology, partial formal analysis (microscopy), JGAS: Conceptualization, Methodology (sample provider), TWM: Conceptualization, Methodology (sample provider), FLT: Conceptualization, Validation, Supervision, Project administration, Funding acquisition. All authors helped to review the manuscript.

**Funding** Open Access funding provided thanks to the CRUE-CSIC agreement with Springer Nature.

## Declarations

**Conflict of interest** The authors declare that they have no known competing financial interests or personal relationships that could have appeared to influence the work reported in this paper.

## References

1. A. Loarte, B. Lipschultz, A. Kukushkin et al., Chapter 4: power and particle control. Nucl. Fusion. **47**, S203–S263 (2007)
2. A. Kallenbach, M. Bernert, R. Dux et al., Impurity seeding for tokamak power exhaust: from present devices via iter to demo. Plasma Phys. Controlled Fusion. **55**, 124041 (2013)
3. B.B. Lipschultz, B. LaBombard, E.S. Marmar et al., Marfe: an edge plasma phenomenon. Nucl. Fusion. **24**, 8 (1984)
4. S.I. Krasheninnikov, A.S. Kukushkin, A.A. Pshenov, Divertor plasma detachment. Phys. Plasmas. **23**, 055602 (2016)
5. H. Reimerdes, R. Ambrosino, P. Innocente et al., Assessment of alternative divertor configurations as an exhaust solution for DEMO. Nucl. Fusion. **60**, 066030 (2020)
6. C.S. Chang, S. Ku, A. Loarte et al., Gyrokinetic projection of the divertor heat-flux width from present tokamaks to ITER. Nucl. Fusion. **57**, 116023 (2017)
7. T. Eich, A.W. Leonard, R.A. Pitts et al., Scaling of the tokamak near the scrape-off layer H-mode power width and implications for ITER. Nucl. Fusion. **53**, 093031 (2013)
8. J. Horacek, J. Cecrdle, D. Tskhakaya et al., Predictive modelling of liquid metal divertor: from COMPASS tokamak towards Upgrade. Phys. Scr. **96**, 124013 (2021)
9. G. Federici, W. Biel, M.R. Gilbert, R. Kemp, N. Taylor, R. Wenninger, European DEMO design strategy and consequences for materials. Nucl. Fusion. **57**, 092002 (2017)
10. J.H. You, C. Bachmann, V.G. Belardi et al., Limiters for DEMO wall protection: initial design concepts & technology options. Fusion Eng. Des. **174**, 112988 (2022)
11. P. Rindt, J.L. van den Eijnden, T.W. Morgan, N.J. Lopes Cardozo, Conceptual design of a liquid-metal divertor for the European DEMO. Fusion Eng. Des. **173**, 112812 (2021)
12. S. Entler, J. Horacek, T. Dlouhy, V. Dostal, Approximation of the economy of fusion energy. Energy. **152**, 489–497 (2017)
13. R.E. Nygren, F.L. Tabares, Liquid surfaces for fusion plasma facing components—a critical review. Part I: physics and PSI. Nucl. Mater. Energy **9**, 6–21 (2016)
14. J.G.A. Scholte, B. Boeswirth, J. Cecrdle, et al., Performance of a liquid tin divertor target during ASDEX Upgrade L and H-mode operation, in *Oral presentation at 7th International Symposium on Liquid Metals Applications for Fusion, Chubu University, 13rd–16th December 2022, Japan*
15. D. Alegre, E. Oyarzábal, D. Tafalla et al., Design and testing of advanced liquid metal targets for DEMO divertor: the OLMAT project. J. Fusion Energy **39**, 411 (2020)
16. F.L. Tabarés, E. Oyarzábal, D. Alegre et al., Commissioning and first results of the OLMAT facility. Fusion Eng. Des. **187**, 113373 (2023)
17. E. Siegel, Optical reflectivity of liquid metals at their melting temperatures. Phys. Chem. Liq. **5**, 9 (1976)
18. W. Ou, R.S. Al, J.V.M. Vernimmen et al., Deuterium retention in Sn-filled samples exposed to fusion-relevant flux plasmas. Nucl. Fusion. **60**, 026008 (2020)
19. C.A. Johnson, D.A. Ennis, S.D. Loch et al., Advances in neutral tungsten ultraviolet spectroscopy for the potential benefit to gross erosion diagnosis. Plasma Phys. Control Fusion. **61**, 095006 (2019)
20. A. Suslova, O. El-Atwani, D. Sagapuram et al., Recrystallization and grain growth induced by ELMs-like transient heat loads in deformed tungsten samples. Sci. Rep. **4**, 6845 (2014)
21. G. Maddaluno, D. Marzullo, G. Mazzitelli et al., The DTT device: divertor solutions for alternative configurations including liquid metals. Fusion Eng. Des. **122**, 341–348 (2017)
22. J. Horacek, S. Entler, P. Vondracek et al., Plans for liquid metal divertor in Tokamak compass. Plasma Phys. Rep. **44**, 652–656 (2018)



## Authors and Affiliations

**A. de Castro[1] · E. Oyarzábal[1] · D. Alegre[1] · D. Tafalla[1] · M. González[1] · K. J. McCarthy[1] · J. G. A. Scholte[2,3] · T. W. Morgan[2,3] · F. L. Tabarés[1] · and the OLMAT team**

✉ A. de Castro
alfonsodcc11@gmail.com

[1] Laboratorio Nacional de Fusión, Av. Complutense, 40, Madrid 28040, Spain

[2] Department of Applied Physics and Science Education, Eindhoven University of Technology, Groene Loper 19, 5612 AP Eindhoven, The Netherlands

[3] DIFFER-Dutch Institute for Fundamental Energy Research, De Zaale 20, 5612 AJ Eindhoven, The Netherlands